RSC Advances

ROYAL SOCIETY OF CHEMISTRY

www.rsc.org/advances

Gel Electrophoresis and Raman Mapping for Determining the Length Distribution of SWCNTs

Waris Obitayo [a], Sida Luo [a], Zhiwei Xiao [a], Tao Liu [a] * and Jingjiao Guan[b]†

TOC

A simple method (GEP-SRSPL) combines gel electrophoresis and simultaneous Raman scattering and photoluminescence spectroscopy for length distribution measurements of SWCNTs.

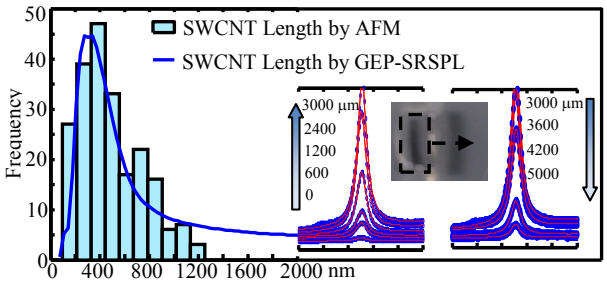

RSC Advances

RSCPublishing

PAPER

Gel Electrophoresis and Raman Mapping for Determining the Length Distribution of SWCNTs

Cite this: DOI: 10.1039/xoxxoooooox

Waris Obitayo [a], Sida Luo [a], Zhiwei Xiao [a], Tao Liu [a] * and Jingjiao Guan[b]†

Received ooth January 2012,
Accepted ooth January 2012

DOI: 10.1039/xoxxoooooox

www.rsc.org/

By combining the gel electrophoresis (GEP) and simultaneous Raman scattering and photoluminescence spectroscopy (SRSPL), a new method (GEP-SRSPL) was established, both theoretically and experimentally, to characterize the length distribution of individualized single-walled carbon nanotubes (SWCNTs). With an individualized SWCNT sample prepared by sonication and ultracentrifugation, both atomic force microscopy (AFM) and GEP-SRSPL were applied for examining its length distribution. The results show good agreement, which validate the GEP-SRSPL method as a viable and easy-to-operate technique in characterizing the length distribution of SWCNTs.

1 Introduction

Single-walled carbon nanotubes (SWCNTs) are quasi-one-dimensional materials with exceptional electronic, optical and mechanical properties [1, 2]. As a result, they have shown great potential for a wide range of applications in areas ranging from micro- and nano-scale electronics [3], thin film sensors [4], lightweight structural nanocomposite materials [5] to biosensors [6, 7]. For most of these emerging applications, the length of SWCNTs is an important structure parameter that affects the physical properties of SWCNTs and thus the SWCNT-based devices. For example, the optical properties and quantum yields [8, 9], electrical and rheological percolation threshold [10-13], and the stress transfer efficiency or mechanical reinforcement in structural nanocomposites [14, 15] all depend on SWCNT length. The progress in the potential use of SWCNTs will rely on the skill to exert control over SWCNT length as well as to develop the corresponding characterization/measurement techniques. To this regard, SWCNT length fractionation has been realized with techniques such as size exclusion chromatography (SEC) [16], flow-field flow fractionation (flow-FFF)[17] , cross flow filtration[18], gel electrophoresis (GEP) [19] and centrifugation [8, 20]. The ability to achieve length-fractionated SWCNTs has enabled the qualitative characterization and understanding of the length-dependent SWCNT properties, such as UV-Vis-NIR [8, 20, 21], Raman scattering [21, 22] and photoluminescence (PL) spectroscopic properties [21, 23, 24]. Furthermore, there are also a variety of different techniques available for quantitative characterization of SWCNT length and/or length distribution. These include the commonly practiced microscopic imaging techniques such as atomic force microscopy (AFM) and transmission electron microscopy (TEM). The size determination based on real-space images is quite appealing for these microscopy methods. Nevertheless, the associated issues, such as time-consuming, subjective and sensitive to sample preparations, are also apparent. The disadvantages of the microscopy technique can be overcome by a few recently developed SWCNT size characterization methods, which include the preparative ultracentrifugation method (PUM) [25], the static and dynamic light scattering techniques [17, 26-28], as well as the simple viscosity measurements [12, 29]. However, most of these techniques provide the reliable information regarding the average length but not the full distribution. Recently, different techniques have been developed to characterize the length distribution of SWCNTs in dispersion [30-32]. For example, Casey et al. used PL to obtain the length distribution of semiconducting-SWCNTs through the study of their highly anisotropic optical properties when aligned by shear flows. A method they termed "shear-aligned photoluminescence anisotropy (LASAPA)" [30]. On the other hand, Streit at al. developed a method called length analysis by nanotube diffusion (LAND) to analyze the diffusional motions of individual SWCNTs in liquids for deriving the information about their length distribution [31]. Pease et al. also invented a method known as differential mobility analysis (DMA) to characterize the length distribution of SWCNTs. In DMA, the SWCNT dispersion was electro-sprayed and then isolated

according to their charge-to-size ratio for length distribution determination [32].

GEP is routinely used in clinical chemistry and biochemistry and molecular biology for separation and analysis of a variety of biological macromolecules [33-35]. The use of GEP for concomitant separation of SWCNT length and diameter was also demonstrated by Heller et al. [19]. Raman scattering spectroscopy (RSS) is an important spectroscopy technique being widely adopted in SWCNT research [21, 22, 36, 37]. In particular, with a commercial RSS instrument and without introducing the complicated instrument correction issues, Liu et al. have shown that the simultaneously acquired Raman scattering and photoluminescence spectra (SRSPL) from SWCNT dispersion can be useful for assessing the quality of SWCNTs in dispersion [38-40], such as the exfoliation efficiency of SWCNT bundles [39], defect density of chemically functionalized SWCNTs [40] as well as the length-dependent photoluminescence quantum yield (PL QY) of an individual semiconducting SWCNT [3, 21, 24]. By taking advantage of the GEP facilitated length fractionation as well as the length dependent PL QY of SWCNTs, we developed a new and simple GEP and RSS combined method – GEP-SRSPL that allows for quantitative measurement of the length distribution of SWCNTs in dispersion. In this paper, we present in details the theoretical basis and the experimental validation and application of the GEP-SRSPL method. As compared to the previously developed techniques, the implementation and practice of GEP-SRSPL are much simpler. The simplicity of GEP-SRSPL relies on its combined use of GEP and RSS, both of which are being commonly practiced in its own field with easy-to-access standardized instrumentation. As a consequence, we expect the newly developed GEP-SRSPL would make the examination of the length distribution of SWCNTs a routine operation in both industrial and academic laboratories.

2. Experimental

2.1 Preparation and Characterization of SWCNT dispersions

By following a previously developed experimental protocol [39, 41, 42], the individualized SWCNT dispersion was prepared for the use to demonstrate the GEP-SRSPL method. In brief, 16 mg purified SWCNTs (Unidym Inc., batch #126) were dispersed in 100 ml of 0.7 wt. % sodium dodecylbenzenesulfonate (SDBS, 99% Sigma-Aldrich, CAS # – 25155-30-10) deionized water solution using a horn sonicator (Misonix sonicator 3000, Frequency 20 KHz) in an ice bath. The sonicator was operated in pulse operation mode (on 10s, off 30s) with the power level set at 45W for 2-hr effective sonication duration. The as-sonicated dispersion (S2hr) was subsequently subjected to centrifugation treatment at 200,000 g-force for 2.45 hrs by Optima^{TM} Max Ultracentrifuge (Becker Coulter, MLS-50 swinging bucket rotor). The supernatant (S2hr-200kg) was then collected in a glass vial and stored at room temperature for later use in length distribution characterization.

For both of the as-sonicated and centrifuged SWCNT dispersion, dynamic light scattering (DLS) was performed with Delsa Nano C particle Size Instrumentation (Beckman Coulter, Inc., scattering angle of 165^o, laser wavelength of 658 nm) to determine the bulk averaged translational diffusion coefficient (D) of SWCNTs at 25^{o}C. By using Optima^{TM} MAX-XP ultracentrifuge operated with a fixed angle rotor (30^0, TLA-100.3) as well as a Varian Cary 5000 UV-Vis-NIR spectrometer, the recently developed preparative ultracentrifuge method (PUM) [25] was applied to determine the sedimentation coefficient (S) for the same sets of dispersion. The bulk-averaged length (L) and bundle diameter (d) were then calculated from the PUM determined S and DLS measured D according to the hydrodynamic model of rigid rods [43]:

$$S = \frac{(\rho_0 - \rho)d^2}{12\eta}\left[ln\left(\frac{L}{d}\right) + 2ln2 - 1\right] \quad \text{Eq. (1)}$$

$$D = \frac{kT}{3\pi\eta L}\left[ln\left(\frac{L}{d}\right) + 2ln2 - 1\right] \quad \text{Eq. (2)}$$

where ρ and ρ_0 are respectively the density of the dispersed particle and the solvent, η is the viscosity of the solvent, k is the Boltzmann constant, and T is the temperature. In the calculation, the values of ρ_0, η and T were taken as 1.0 g/cm^3, 0.890 dyne.sec/cm^2, and 298 K respectively. According to our recent studies [44], the SWCNT density ρ was respectively taken as 1.20 and 1.07 g/cm^3 for the as-sonicated and individualized SWCNT dispersion respectively.

High-resolution transmission electron microscopy (HR-TEM, JEM–ARM200cF, JEOL Ltd. was applied for qualitative examination of the morphologies of SWCNTs. The TEM sample was prepared by drop casting and drying SWCNT dispersion on a Lacey grid (300 mesh Cu: Ted Pella). The tapping mode AFM (Veeco Instruments, Inc. Multimode) was used to acquire images of the individualized SWCNTs on a silicon wafer substrate under ambient conditions to determine the length distribution and validate the GEP-SRSPL results.

2.2 Gel Electrophoresis of SWCNTs mapped by Simultaneous Raman scattering and Photoluminescence spectroscopy

Agarose gel with fixed solid content of 0.7 wt. % was prepared for performing the gel electrophoresis of SWCNT dispersion. In brief, 1.05 grams of agarose powder (BE A500, LOT# -12D2005, MIDSCI – Laboratory Equipment & Supplies) was dissolved in 150 ml of 0.7 wt. % SDBS aqueous solution by magnetic stirring at elevated temperature. The clear agarose solution was subsequently cooled to 55^{o}C and then poured into a gel casting tray (15 cm × 10 cm) for further cooling and gel formation. During this process, a comb template was inserted for forming sample loading well. To perform the gel electrophoresis of SWCNT dispersion, the fully gelled agarose slab was carefully placed into the electrophoresis chamber (17.5 cm × 26.5 cm gel tank, E1015-10-GT - VMR® Midi plus Horizontal Electrophoresis system), in which 400ml of 0.7 wt. % SDBS aqueous solution was filled as the buffer solution. In a typical electrophoresis run, 100 µl of S2hr-200kg

dispersion was loaded and subjected to a constant electric field of 10V/26 cm = 0.385 V/cm for 1 hr. Varied field strength was also examined to verify that, with this field strength setting, the electrophoresis mobility of SWCNTs is field-independent. Immediately after the electrophoresis, the gel sample was then cut into a small block (2.5cm × 1.5cm× 1.0cm) for mapping the Raman scattering spectra of electrophoresed SWCNTs with a Reinshaw inVia Raman microscope. The Raman mapping process was facilitated by a computer-controlled motorized XYZ sample stage that has a step resolution of 1 μm. The gel block, which was supported by a glass slide and mounted on the XYZ stage, was mapped along the electrophoresis trace with the sample well as the origin and equal spaced interval (200 μm per spectrum) for simultaneous collection of the Raman scattering and PL emission spectra of electrophoresed SWCNTs. The spectra were collected in backscattering geometry by a 5× objective with a 785 nm (1.58 eV) diode laser as the excitation source. The beam size was approximately 100 μm × 150 μm. For each mapping process, a small-sized silicon wafer was positioned beside the sample well as a reference for facilitating laser beam focus. No attempt was taken to re-adjust the focus during the mapping process. This is critical for eliminating the optics change induced intensity variation so that one can directly associate the detected Raman and PL intensity to the SWCNT concentration. The experimental procedure for SRSPL mapping was validated by mapping the Raman spectra of a silicon wafer placed on a cut gel block. Figure 1 shows the integrated intensity of the 520 cm^{-1} Raman band of the silicon wafer at a series of discrete points along the mapping distance. Over the entire mapping range, the relative variation of the intensity was found to be 1.8 %, which confirms the mapping protocols described above.

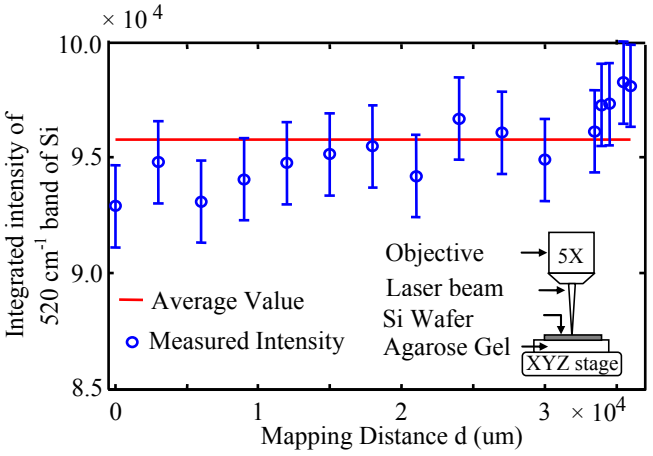

Figure 1. Validation of the experimental procedure for SRSPL mapping of the gel electrophoresed SWCNTs by using the integrated intensity of the 520 cm^{-1} Raman band of Si acquired along the mapping distance (Error bar: 1 standard deviation). The inset schematically shows the mapping setup.

3. Results and Discussions

3.1 Structural Characterization of SWCNT dispersion

The PUM method has been proved to be useful and reliable in characterizing the structures of SWCNT dispersions to establish the related processing-structure-property relationships [45-47]. The key of the PUM is the sedimentation function, which is defined as a measure of the time change of SWCNT concentration in a control volume of the dispersion when it is subjected to centrifugation process [25]. According to the decay behavior of the sedimentation function with respect to the centrifugation time at a specific g-force, one can quantitatively infer the sedimentation coefficient S of SWCNTs and therefore, the particle size by theoretically fitting the sedimentation model derived by Mason and Weaver [48]. Figure 2a compares the experimentally determined and theoretically fitted sedimentation function for the as-sonicated (S2hr) and individualized (S2hr-200kg) SWCNT dispersion. The fitted results of the sedimentation coefficients (S) and the diffusion coefficients (D) measured by DLS for both S2hr and S2hr-200kg are listed in Table 1. With the sedimentation coefficient S and diffusion coefficient D determined from PUM and DLS respectively, the bulk average length (L) and bundle diameter (d) were calculated using equation 1 and 2. The results are also listed in Table 1. The structural parameters listed in Table 1 and the sedimentation function shown in Figure 2a both indicate that, upon 200,000 g-force centrifugation for ~ 3 hrs, the large sized SWCNT bundles have been successfully removed from S2hr to leave S2hr-200kg sample enriched with individual tubes. The UV-vis-NIR spectra, which have been shown to be sensitive to the bundling states of SWCNTs [3], were collected to further confirm this point. Figure 2b compares the UV-vis-NIR spectra of the as-sonicated and the individualized SWCNTs. Clearly, the spectrum of the as-sonicated dispersion (S2hr) is featured by the broadened peak features, which are attributed to the intertube interactions existing in a thick SWCNT bundle [49]. In contrast, the well resolved sharp peaks observed for S2hr-200kg indicate the dominance of the individualized tubes in this sample. The TEM images shown in Figure 2c provide additional evidence to show that the individualized SWCNT dispersion (S2hr-200kg) is indeed enriched with individual tubes and small sized SWCNT bundles; and the as-sonicated dispersion (S2hr) is dominated by large-sized SWCNT bundles. AFM was performed to estimate the length distribution of the individualized SWCNT dispersion (S2hr-200kg). Figure 2d shows the histogram of the length distribution that was acquired based upon 400 different measurements. As can be seen in Figure 2d, the SWCNT length distribution of S2hr-200kg can be nicely fitted by a lognormal distribution with mean value of 489.5 nm and standard deviation of 290.5 nm. Some previous work [31] also identified the lognormal length distribution of the SWCNTs that were prepared by the similar protocols used in this study. One notes that the SWCNT length determined by AFM for S2hr-200kg is significantly lower than that obtained by PUM method (Table 1). The discrepancy is attributed to that, for a given length distribution $g(L)$, the mean value provided by the AFM is a number-averaged quantity - $< L >_n = \int Lg(L) / \int g(L)$ and that obtained from the sedimentation based PUM method is a weight-averaged $< L >_w = \int L^2 g(L) / \int Lg(L)$ quantity [50]. According to the previously obtained lognormal distribution parameters for S2hr-200kg (mean = 489.5 nm and standard deviation of 290.5 nm), we can correspondingly estimate the value of $< L >_w$ as 662.6

nm, which shows a reasonable agreement with the PUM result as listed in Table 1.

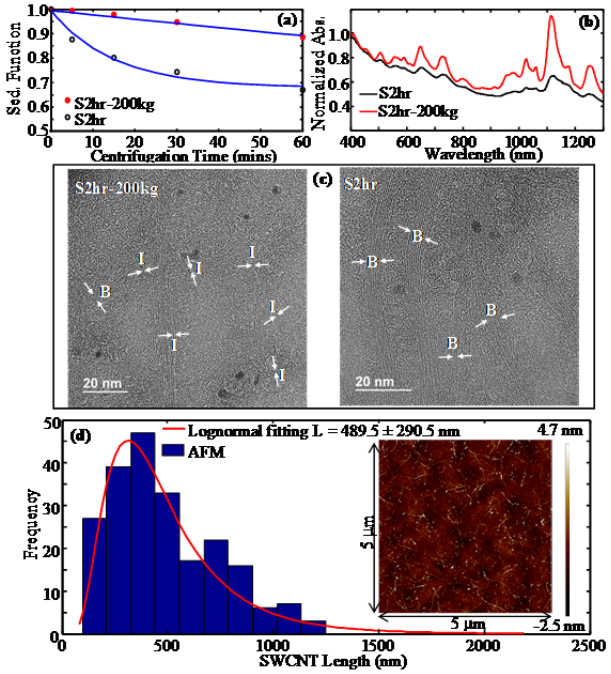

Figure 2. (a) Experimentally determined (scattered data) and theoretically fitted (smooth lines) sedimentation functions for the as-sonicated (S2hr) and the individualized (S2hr-200kg) SWCNT dispersion respectively acquired at a centrifugation field of 13,000g and 65,000g; (b) UV-vis-NIR absorption spectra of S2hr and S2hr-200kg SWCNT dispersion (absorbance is normalized by the value at 400 nm); (c) TEM images of S2hr-200kg and S2hr SWCNT samples. B is for bundle and I is for individual tube. (d) AFM results for the length distribution of the individualized SWCNT sample - S2hr-200kg.

Table 1. Summary of the structural parameters of the as-sonicated (S2hr) and the individualized (S2hr-200kg) SWCNT dispersion characterized by PUM and DLS methods

Sample	Sed. Coeff. (S) ($\times 10^{-13}$ sec)	Diff. Coeff. (D) ($\times 10^{-8}$ cm^2/sec)	Len. (L) (nm)	Dia. (d) (nm)
S2hr	242.1	0.84 ± 0.05	3400.9	14.9
S2hr-200kg	3.68	3.6 ± 0.5	832.8	3.1

3.2 Mobility Distribution of SWCNTs Determined by Raman Mapping and Gel Electrophoresis

GEP has been proved to be a viable technique to sort SWCNTs by lengths[19]. Under the influence of an applied electric field, the SWCNTs of longer length have difficulty traveling through the gel and show small mobility; while the SWCNTs of shorter lengths migrate through the gel faster and have large mobility. The electrophoretic mobility μ is defined as the migration speed V_m under unit electric field strength. With this definition, the SWCNT length-dependent mobility, μ, measured along the electrophoresis trace from the edge of the loading well at distance d is given by:

$$\mu(L) = \frac{V_m}{E} = \frac{d}{Et} \qquad \text{Eq. (3)}$$

where t is the time duration of the electrophoresis process and the typical setting in our experiments is 1 hr.; and E is the constant field strength. The inset of Figure 3 shows a photograph of the electrophoresis trace of the S2hr-200kg dispersion. The broad dark band observed in Figure 3a suggests the sample S2hr-200kg has a broad SWCNT length distribution. In the electrophoresis direction indicated by the dashed-line arrow, the SWCNTs with shorter length/higher mobility are located in the front of the band and the SWCNTs with longer length/smaller mobility are present in the rear of the band. The mobility distribution f (μ) of SWCNTs can be obtained by mapping the SWCNT concentration along the electrophoresis trace. This was performed by using the simultaneous Raman scattering and photoluminescence (SRSPL) spectroscopy as detailed in the experimental section.

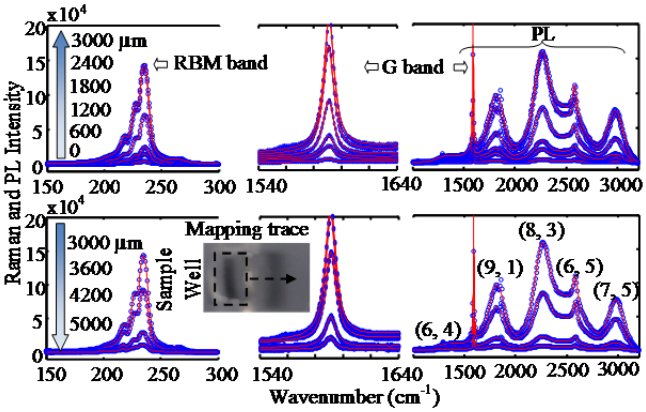

Figure 3. SRSPL spectra of S2hr-200kg mapped along the electrophoresis trace at different distances. The PL emission band of (6, 5) tube is superposed with the Raman G' band (2577 cm^{-1}). The inset is the photograph of the individualized SWCNTs (S2hr-200kg) experienced gel electrophoresis in agarose for 1hr at an electric field of 0.385 V/cm.

The experimentally acquired SRSPL spectra at discrete distances along the electrophoresis trace for S2hr-200kg are shown in Figure 3b and represented by the circle symbols. The continuous lines represent the peak-resolved spectra obtained by peak-fitting performed with the GRAMS/AI spectroscopy software (Thermo Scientific). Clearly, the intensity of the PL features, which are located around 1318 cm^{-1}, 1802 cm^{-1}, 2161 cm^{-1}, 2395 cm^{-1}, and 2883 cm^{-1} and corresponds to the PL emission by (7,5), (6,5), (8,3), (9,1), and (6,4) tubes [39], as well as that of the Raman RBM (radial breathing mode located in the range of 150 – 300 cm^{-1}) and G-bands (1590 cm^{-1}) all show a very similar dependence on the mapping distance. With increasing the distance from the edge of the sample

loading well, the PL and Raman intensity monotonically increases to reach a maximum at ~ 3000 μm, and then it gradually decrease to approach zero.

Considering that the PL and Raman intensity is proportional to the SWCNT concentration, the mobility distribution $f(\mu)$ of the SWCNTs can then be quantified according to the mapped SRSPL intensity by using the distance-mobility relation as given in Eq. (3). The RBM-band, G-band, and PL features all can be used for calculating the $f(\mu)$ and result in the same result if the respective integrated intensity (with respect to the mapping distance) is appropriately used as the normalization factor. Figure 4 shows the averaged result of $f(\mu)$ for S2hr-200kg determined from all these three different bands. It shows a bell-shaped distribution slightly weighted on the low mobility side. It should be noted that, the PL quantum yield of SWCNTs has a strong dependence on the tube length [21, 57, 58]. The shorter is the length, the smaller is the PL quantum yield. This effect creates a difficulty in determining the mobility distribution $f(\mu)$ by mapping the PL intensity, since the latter quantity is a function of both the SWCNT concentration and the quantum yield (Eq. 9b). As a consequence, the $f(\mu)$ would be under-estimated with increasing the mobility. However, such a complication does not exist in Raman scattering intensity mapping, since the Raman scattering cross section of SWCNTs has a weak or negligible dependence on the tube length. This is because the Raman scattering of SWCNTs is mostly determined by the local vibration of the carbon bond structures [1]. As a result, the Raman intensity (Eq. 9a) is simply proportional to the SWCNT concentration and therefore allows for a reliable estimation of the mobility distribution $f(\mu)$.

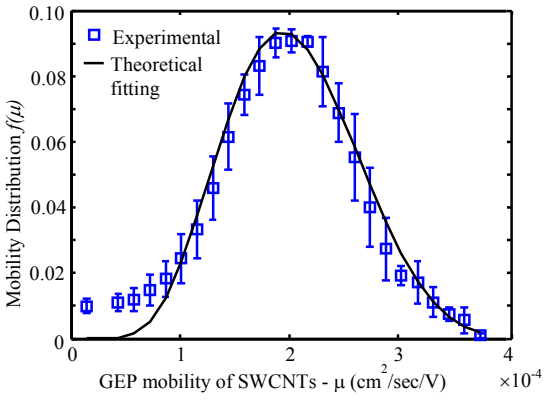

Figure 4. The SWCNT mobility distribution $f(\mu)$ of the sample S2hr-200kg derived from the GEP-SRSPL mapped Raman intensity for the RBM-band, the G-band, and sum of the PL features. The scattered data are the experimental results. The smooth curve is a theoretically fitted result by considering the mobility-length relationship of $1/\mu = A + BL$ and the lognormal distribution - $g(L)$ of the SWCNT length determined by AFM measurements. The fitting parameters are A = 1985.3 and B = 10.2.

To derive the length distribution $g(L)$ from $f(\mu)$, a functional relationship between μ and L for the SWCNTs is necessary, which, unfortunately, is lacking in the open literature. Given such difficulty, we attempted in the present work a simple empirical function

$$\frac{1}{\mu(L)} = A + BL \qquad \text{Eq. (4)}$$

to correlate the GEP mobility μ of the SWCNT to its length L, where the coefficients A and B take into account the effect of charge density of SWCNTs, gel composition and structures, and SWCNT/gel interactions. Qualitatively, Eq. (4) is consistent with the experimental observation on the sorting of SWCNT length by GEP technique [19]. Namely, the SWCNTs of longer length travel through the gel with a smaller mobility. Moreover, the μ - L relation in Eq. (4) has been successfully used to describe the length dependent GEP mobility for a variety of biopolymers, such as DNAs with a broad range of length [34],[35],[51] as well as the rod-like bacteriophage fd (length varied from 367 nm to 2808 nm) [52]. The theoretical basis of Eq. (4) in explaining the μ - L relation of DNA has been attributed to the reptation of DNA through a porous gel structure [53, 54]. The same mechanism also dictates the dynamics of rodlike particles in a polymer liquid [55, 56] which is the case for the gel electrophoresis of SWCNTs in agarose. In the sense of reptation, it seems that the relation given by Eq. (4) that has been tested for DNAs should also be applicable to SWCNTs. Lastly, the appropriateness of Eq. (4) in describing the μ - L relation of SWCNTs can be examined by comparing the $f(\mu)$ of S2hr-200kg determined by GEP-SRSPL with the one derived from its length distribution $g(L)$ as measured by AFM. With the lognormal distribution (mean value of 489.5 nm and standard deviation of 290.5 nm) determined by AFM for S2hr-200kg, we can accordingly derive its mobility distribution $f(\mu)$ by using Eq. (4). By setting the parameters A = 1985.3 and B = 10.2, the best fitted $f(\mu)$ for S2hr-200kg derived from the AFM length distribution was obtained. The result is shown in Figure 4. Clearly, except for the small portion of the distribution at low mobility end, the $f(\mu)$ derived from the AFM measurement agrees reasonably well with that directly measured by GEP-SRSPL. This agreement further confirms Eq. (4) as a useful and reasonable tool in describing the μ - L relationship for the GEP of SWCNTs. With this relation, the length distribution can be derived from the GEP mobility distribution $f(\mu)$, if the values of A and B are known. In the next section, we will present an in-depth analysis to show how A and B can be estimated from the GEP-SRSPL spectra by utilizing a previously developed analytical relationship between the SWCNT length and its PL quantum yield [40].

3.3 GEP-SRSPL for Determining the Length Distribution of SWCNTs

(a) Intensity of Raman scattering and photoluminescence in SRSPL – a theoretical derivation

As demonstrated in our previous work [39] and shown by Eq. (5), the advantage of using SRSPL to characterize SWCNT dispersion is that one can readily acquire the valued information about the intrinsic optical absorption cross section - ε, Raman scattering cross section - β, and PL quantum yield ϕ of SWCNTs

through a ratio of the intensity of a PL band - I_{PL} to that of a Raman band, e.g., G-band - I_G.

$$\frac{I_{PL}}{I_G} = \frac{\varepsilon\phi}{\beta} \quad \text{Eq. (5)}$$

The derivation of Eq. (5) has not been disclosed in [39] and will be provided as following .

We consider an incident laser beam of intensity I_0 propagates from air into a SWCNT dispersion/gel sample of concentration C. As schematically shown in Figure 5, at a distance x from the sample surface, the beam intensity attenuates to $I_0(x)$ due to absorption and it is given by the well-known Lambert-Beer law:

$$I_0(x) = I_0 exp(-\varepsilon C x) \quad \text{Eq. (6)}$$

Denote $\delta I_s(x)$ and $\delta I_{PL}(x)$ as the differential Raman and PL intensity respectively scattered and emitted by SWCNTs that are located between x and $x + \delta x$ and excited by $I_0(x)$. Then, according to the definition of β - Raman scattering cross section and ϕ - PL quantum yield, we have:

$$\delta I_s(x) = I_0(x)\beta C \delta x \quad \text{Eq. (7a)}$$

$$\delta I_{PL}(x) = I_0(x)[1 - exp(-\varepsilon C \delta x)]\phi = I_0(x)\varepsilon C \delta x \quad \text{Eq. (7b)}$$

It is noted that $\delta I_s(x)$ and $\delta I_{PL}(x)$ are subjected to further attenuation before reaching the optical detection system. By taking into account the re-absorption issue and using Eq. (6), the differential scattered and emitted intensity $\delta I_{s-d}(x)$ and $\delta I_{PL-d}(x)$ recorded by the detector is accordingly re-written as:

$$\delta I_{s-d}(x) = \delta I_s(x) exp(-\varepsilon C x) K = I_0 K \beta C exp(-2\varepsilon C x)\delta x \quad \text{Eq. (8a)}$$

$$\delta I_{PL-d}(x) = \delta I_{PL}(x) exp(-\varepsilon C x) K = I_0 K \varepsilon C \phi exp(-2\varepsilon C x)\delta x \quad \text{Eq. (8b)}$$

The constant K in Eq. (8a) and 8(b) takes into account the instrumentation factor in measuring the light intensity, which is the same for both Raman scattering and PL emission in SRSPL.

Let H be the sampling depth of a given measurement, then an integration of Eq. (8a) and (8b) from 0 to H gives the total detected Raman and PL intensity. They are:

$$I_{Raman} = \int_0^H \delta I_{s-d}(x) = \frac{K I_0 \beta}{2\varepsilon}[1 - exp(-2\varepsilon C H)] \approx K I_0 \beta C H \quad \text{Eq. (9a)}$$

$$I_{PL} = \int_0^H \delta I_{PL-d}(x) = \frac{K I_0 \phi}{2}[1 - exp(-2\varepsilon C H)] \approx K I_0 \phi \varepsilon C H \quad \text{Eq. (9b)}$$

Eq. (5) is then recovered by taking the ratio of I_{PL} to I_{Raman}. The last equality in Eq. (9a) and (9b) is an approximation when the SWCNT concentration is low.

(b) Determination of the coefficient A and B in the μ-L relationship by GEP-SRSPL

It has been well established that the PL quantum yield of SWCNT - ϕ strongly depends on the tube length and its internal defect density [21, 57, 58]. A closed-form solution of ϕ for a defective SWCNT of finite length L has been developed in our previous work [40], which is given by Eq. (10):

$$\phi = \phi(\infty, 0)\left\{1 - 2\nu_n\left[ln\frac{\nu_n}{2} + 2ln\frac{\Gamma\left(\frac{\nu_n}{2}\right)}{\Gamma\left(\frac{\nu_n+1}{2}\right)}\right]\right\}, \nu_n = l_\infty\left(m + \frac{1}{L}\right) \quad \text{Eq. (10)}$$

where ϕ (∞, 0) represents the intrinsic PL quantum yield of a SWCNT with infinite length and zero defect density; ν_n is a parameter to characterize the defect density, in which l_∞ is the exciton diffusion length, m is the number density of the internal defects associated with a given SWCNT, and $1/L$ accounts for one defect formed by the two ends the SWCNT of finite length. Substitute Eq. (10) into Eq. (5) and use the established μ-L relation Eq. (4), we then have

$$\frac{I_{PL}}{I_G} = \frac{\epsilon\phi(\infty,0)}{\beta}\left\{1 - 2\nu_n\left[ln\frac{\nu_n}{2} + 2ln\frac{\Gamma\left(\frac{\nu_n}{2}\right)}{\Gamma\left(\frac{\nu_n+1}{2}\right)}\right]\right\}, \nu_n = l_\infty\left(m + \frac{B\mu}{1-A\mu}\right) \quad \text{Eq. (11a)}$$

By defining $P_1 = \frac{\epsilon\phi(\infty,0)}{\beta}, P_2 = l_\infty m$, $P_3 = l_\infty B$ and $P_4 = A$, Eq. (11a) can be re-written as a four- parameter equation:

$$\frac{I_{PL}}{I_G} = P_1\left\{1 - 2\nu_n\left[ln\frac{\nu_n}{2} + 2ln\frac{\Gamma\left(\frac{\nu_n}{2}\right)}{\Gamma\left(\frac{\nu_n+1}{2}\right)}\right]\right\}, \nu_n = P_2 + \frac{P_3\mu}{1-P_4\mu} \quad \text{Eq. (11b)}$$

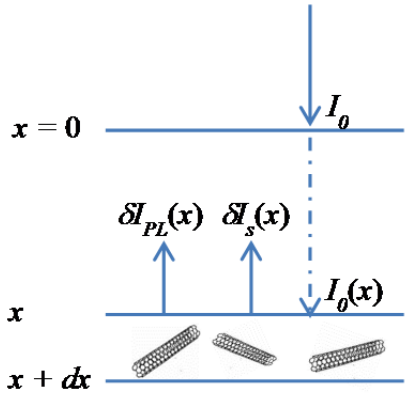

Figure 5. A schematic diagram for deriving Eq. (5) to show the process of absorption, PL emission and Raman scattering of SWCNTs in a dispersion sample. I_0 is the intensity of the incident laser beam at $x = 0$ (sample/air interface); $I_0(x)$ is the intensity of the laser beam at distance x into the sample; $\delta I_s(x)$ and $\delta I_{PL}(x)$ are the differential Raman and PL intensity respectively scattered and emitted by SWCNTs that are located between x and $x + \delta x$ and excited by $I_0(x)$.

As a consequence of the relation between the PL quantum yield ϕ of a SWCNT and its length L – the shorter is the L, the smaller is the ϕ, Eq. (11a) or 11(b) predicts a monotonically decreasing behavior of the I_{PL}/I_G with increasing μ. Clearly, by fitting the experimentally measured data set of μ vs. I_{PL}/I_G through GEP-SRSPL, the four unknown parameters P_1 – P_4 can be determined, from which the coefficients A and B of the μ - L relation can be accordingly derived as $A = P_4$ and $B = P_3/l_\infty$. Eq. (11b) was applied to fit μ vs. $I_{PL\text{-}SUM}/I_G$ results of the S2hr-200kg sample

acquired from the GEP-SRSPL spectra, where $I_{PL\text{-}SUM}$ is the intensity summed over all the five PL bands as shown in Figure 3. With the peak-fitting procedures, one can also use the individually resolved PL bands to calculate $I_{PL\text{-}(n,m)}/I_G$ for a specific (n, m) tube. The advantage of using $I_{PL\text{-}SUM}$ over $I_{PL\text{-}(n,m)}$ is to avoid the uncertainties/ambiguities involved in the peak fitting process. Figure 6a shows the experimentally determined μ vs. $I_{PL\text{-}SUM}/I_G$ for S2hr-200kg averaged over three repeating GEP runs.

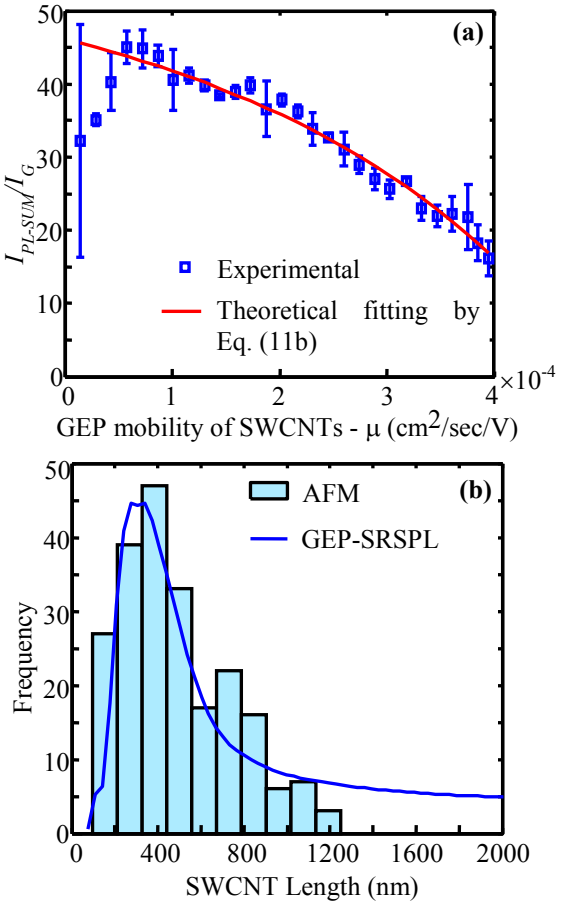

Figure 6. (a) Relationship between the GEP mobility and the G-band normalized PL intensity – $I_{PL\text{-}SUM}/I_G$ for S2hr-200kg sample: the experimental results versus theoretical fitting according to Eq. (11). The fitting parameters are: P_1 = 656.3, P_2 = 1.254, P_3 = 714.7, and P_4 = 1875.1 b) A comparison of the length distribution of S2hr-200kg measured by AFM and calculated according to its mobility distribution determined by GEP-SRSPL through using the μ - L relationship with the coefficient A = 1875.1 and B = 10.2.

As shown in Figure 6a, one notes an initial increasing trend of the $I_{PL\text{-}SUM}/I_G$ with μ. This is a result of the presence of small amount of SWCNT bundles in the S2hr-200kg sample (Figure 2c). Due to bundling, the PL emission of SWCNTs can be quenched to cause the reduced PL intensity and therefore the value of $I_{PL\text{-}SUM}/I_G$ [39]. With exclusion of the few data points at small values of μ, the μ vs. $I_{PL\text{-}SUM}/I_G$ for s2hr-200kg was fitted according to Eq. (11b) and the results are shown in Figure 6a. The coefficient A obtained by fitting the GEP-SRSPL spectra is 1875.1, which agrees very well with the value of A = 1958.3 determine by AFM measurements (Figure 4). Such agreement further confirms the validity of μ - L relationship as described by Eq. (4) and the usefulness of Eq. (11) in extracting the structural parameters of SWCNT by using the GEP-SRSPL technique. This point can be further strengthened by a good agreement between the length distribution of S2hr-200kg determined by AFM and the one calculated according to its mobility distribution through using the μ - L relationship with the coefficient A = 1875.1 and B = 10.2. The result is shown in Figure 6b. By using the coefficient B = 10.2 determined from the AFM measurement and the parameter P_3 = 714.7 obtained through fitting the GEP-SRSPL spectra, the exciton diffusion length l_∞ was calculated to be $l_\infty = P_3/B$ = 70.1 nm. This value is ~ 3 × smaller than that reported in the literature [40, 59]. The reason for such a low value of l_∞ is not clear, but it is presumably related to the relatively high defect density m of the S2hr-200kg sample, which is estimated by $P_2 \times B/P_3$ = 1.254×10.2/714.7 = 0.018/nm.

4. Conclusions

By taking advantage of the length fractionation of SWCNTs in gel electrophoresis (GEP) as well as the previously established relationship between the photoluminescence (PL) quantum yield and the SWCNT length, the present work established, both theoretically and experimentally, a new method – combined gel electrophoresis and simultaneous Raman scattering and photoluminescence spectroscopy (GEP-SRSPL) to allow for the determination of the length distributions of an individualized SWCNT sample. The conventional atomic force microscopy (AFM) and the newly developed GEP-SRSPL method were applied to examine the length distribution of an individualized SWCNT sample prepared by sonication and ultracentrifugation. The results show good agreement, which confirms the GEP-SRSPL method as a viable and easy-to-operate technique in characterizing the length distribution of SWCNTs.

Acknowledgements

W. Obitayo, S. Luo, and T. Liu acknowledge the funding support provided by the Air Force Office of Scientific Research (AFOSR) and supervised by Dr. David S. Stargel.

AUTHOR INFORMATION
Corresponding Author
*T. Liu[1], liutao@eng.fsu.edu, †J. Guan[2], guan@eng.fsu.edu,

[1] High-Performance Materials Institute, Florida State University, Tallahassee, FL 32310, USA
[2] Department of Chemical and Biomedical Engineering, FAMU-FSU College of Engineering, Florida State University, Tallahassee, FL 32310, USA

Notes and references

1. Dresselhaus M. S., D.G.A.P., *Carbon Nanotubes Synthesis, Structure, Properties, and Applications* 2001: Springer.
2. Baughman, R.H., A.A. Zakhidov, and W.A. de Heer, *Carbon Nanotubes--the Route Toward Applications.* Science, 2002. **297**(5582): p. 787-792.
3. O'Connell, M.J., et al., *Band Gap Fluorescence from Individual Single-Walled Carbon Nanotubes.* Science, 2002. **297**(5581): p. 593-596.
4. Barone, P.W., et al., *Near-infrared optical sensors based on single-walled carbon nanotubes.* Nat Mater, 2005. **4**(1): p. 86-92.
5. Clayton, L.M., et al., *Transparent Poly(methyl methacrylate)/Single-Walled Carbon Nanotube (PMMA/SWNT) Composite Films with Increased Dielectric Constants.* Advanced Functional Materials, 2005. **15**(1): p. 101-106.
6. Naveen R Palwai, D.E.M., Luis F F Neves, Yongqiang Tan, Daniel E Resasco and Roger G Harrison, *Retention of biological activity and near-infrared absorbance upon adsorption of horseradish peroxidase on single-walled carbon nanotubes.* Nanotechnology, 2207. **2218**: p. 23.
7. Lin, J.W.a.Y., *Functionalized carbon nanotubes and nanofibers for biosensing applications.* Analyt Chem, 2008. **27**(7): p. 619-626.
8. Fagan, J.A., et al., *Length Fractionation of Carbon Nanotubes Using Centrifugation.* Advanced Materials, 2008. **20**(9): p. 1609-1613.
9. Crochet, J., M. Clemens, and T. Hertel, *Quantum Yield Heterogeneities of Aqueous Single-Wall Carbon Nanotube Suspensions.* Journal of the American Chemical Society, 2007. **129**(26): p. 8058-8059.
10. Balberg, I., N. Binenbaum, and N. Wagner, *Percolation Thresholds in the Three-Dimensional Sticks System.* Physical Review Letters, 1984. **52**(17): p. 1465-1468.
11. Kyrylyuk, A.V. and P. van der Schoot, *Continuum percolation of carbon nanotubes in polymeric and colloidal media.* Proceedings of the National Academy of Sciences, 2008. **105**(24): p. 8221-8226.
12. Davis, V.A., et al., *Phase Behavior and Rheology of SWNTs in Superacids.* Macromolecules, 2003. **37**(1): p. 154-160.
13. Abu-Abdeen, M., A.S. Ayesh, and A.A. Aljaafari, *Dielectric relaxation and rheological properties of single walled carbon nanotubes reinforced poly(3-octylthiophene-2,5-diyl).* Journal of Thermoplastic Composite Materials, 2011.
14. Thostenson, E.T., Z. Ren, and T.W. Chou, *Advances in the science and technology of carbon nanotubes and their composites: a review.* Composites Science and Technology, 2001. **61**(13): p. 1899-1912.
15. Cadek, M., et al., *Reinforcement of Polymers with Carbon Nanotubes: The Role of Nanotube Surface Area.* Nano Letters, 2004. **4**(2): p. 353-356.
16. Huang, X., R.S. McLean, and M. Zheng, *High-Resolution Length Sorting and Purification of DNA-Wrapped Carbon Nanotubes by Size-Exclusion Chromatography.* Analytical Chemistry, 2005. **77**(19): p. 6225-6228.
17. Chun, J., et al., *Size Separation of Single-Wall Carbon Nanotubes by Flow-Field Flow Fractionation.* Analytical Chemistry, 2008. **80**(7): p. 2514-2523.
18. Ohmori, S., et al., *Fractionation of Single Wall Carbon Nanotubes by Length Using Cross Flow Filtration Method.* ACS Nano, 2010. **4**(7): p. 3606-3610.
19. Heller, D.A., et al., *Concomitant Length and Diameter Separation of Single-Walled Carbon Nanotubes.* Journal of the American Chemical Society, 2004. **126**(44): p. 14567-14573.
20. Fagan, J.A., et al., *Centrifugal Length Separation of Carbon Nanotubes.* Langmuir, 2008. **24**(24): p. 13880-13889.
21. Fagan, J.A., et al., *Length-Dependent Optical Effects in Single-Wall Carbon Nanotubes.* Journal of the American

Chemical Society, 2007. **129**(34): p. 10607-10612.
22. Chou, S.G., et al., *Length characterization of DNA-wrapped carbon nanotubes using Raman spectroscopy.* Applied Physics Letters, 2007. **90**(13): p. 131109-3.
23. Cherukuri, T.K., D.A. Tsyboulski, and R.B. Weisman, *Length- and Defect-Dependent Fluorescence Efficiencies of Individual Single-Walled Carbon Nanotubes.* ACS Nano, 2011. **6**(1): p. 843-850.
24. Miyauchi, Y., et al., *Length-Dependent Photoluminescence Lifetimes in Single-Walled Carbon Nanotubes.* The Journal of Physical Chemistry C, 2010. **114**(30): p. 12905-12908.
25. Liu, T., et al., *Preparative Ultracentrifuge Method for Characterization of Carbon Nanotube Dispersions.* The Journal of Physical Chemistry C, 2008. **112**(49): p. 19193-19202.
26. Badaire, S., et al., *In Situ Measurements of Nanotube Dimensions in Suspensions by Depolarized Dynamic Light Scattering.* Langmuir, 2004. **20**(24): p. 10367-10370.
27. Ji Yeong Lee, J.S.K., Kay Hyeok An,Kyu Lee,Dong Young Kim,Dong Jae Bae,and Young Hee Lee, *Electrophoretic and Dynamic Light Scattering in Evaluating Dispersion and Size Distribution of Single-Walled Carbon Nanotubes.* Journal of Nanoscience and Nanotechnology, 2005. **5**: p. 1045-1049.
28. Shetty, A.M., et al., *Multiangle Depolarized Dynamic Light Scattering of Short Functionalized Single-Walled Carbon Nanotubes.* The Journal of Physical Chemistry C, 2009. **113**(17): p. 7129-7133.
29. Parra-Vasquez, A.N.G., et al., *Simple Length Determination of Single-Walled Carbon Nanotubes by Viscosity Measurements in Dilute Suspensions.* Macromolecules, 2007. **40**(11): p. 4043-4047.
30. Casey, J.P., et al., *Chirality-Resolved Length Analysis of Single-Walled Carbon Nanotube Samples through Shear-Aligned Photoluminescence Anisotropy.* ACS Nano, 2008. **2**(8): p. 1738-1746.
31. Streit, J.K., et al., *Measuring Single-Walled Carbon Nanotube Length Distributions from Diffusional Trajectories.* ACS Nano, 2012. **6**(9): p. 8424-8431.
32. Pease, L.F., 3rd, et al., *Length distribution of single-walled carbon nanotubes in aqueous suspension measured by electrospray differential mobility analysis.* Small, 2009. **5**(24): p. 2894-901.
33. Elson, E. and T.M. Jovin, *Fractionation of oligodeoxynucleotides by polyacrylamide gel electrophoresis.* Analytical Biochemistry, 1969. **27**(2): p. 193-204.
34. Van Winkle, D.H., A. Beheshti, and R.L. Rill, *DNA electrophoresis in agarose gels: A simple relation describing the length dependence of mobility.* ELECTROPHORESIS, 2002. **23**(1): p. 15-19.
35. Elder, J.K., et al., *Measurement of DNA length by gel electrophoresis: I. Improved accuracy of mobility measurements using a digital microdensitometer and computer processing.* Analytical Biochemistry, 1983. **128**(1): p. 223-226.
36. Izard, N., D. Riehl, and E. Anglaret, *Exfoliation of single-wall carbon nanotubes in aqueous surfactant suspensions: A Raman study.* Physical Review B, 2005. **71**(19): p. 195417.
37. O'Connell, M.J., S. Sivaram, and S.K. Doorn, *Near-infrared resonance Raman excitation profile studies of single-walled carbon nanotube intertube interactions: A direct comparison of bundled and individually dispersed HiPco nanotubes.* Physical Review B, 2004. **69**(23): p. 235415.
38. Kono, K., et al., *Simultaneous measurement of photoluminescence and Raman scattering spectra from suspended single-walled carbon nanotubes.* Surface and Interface Analysis, 2012. **44**(6): p. 686-689.
39. Liu, T., Z. Xiao, and B. Wang, *The exfoliation of SWCNT bundles examined by simultaneous Raman scattering and*

photoluminescence spectroscopy. Carbon, 2009. **47**(15): p. 3529-3537.
40. Liu, T. and Z. Xiao, *Exact and Closed Form Solutions for the Quantum Yield, Exciton Diffusion Length, and Lifetime To Reveal the Universal Behaviors of the Photoluminescence of Defective Single-Walled Carbon Nanotubes*. The Journal of Physical Chemistry C, 2011. **115**(34): p. 16920-16927.
41. Nair, N., et al., *Dynamics of Surfactant-Suspended Single-Walled Carbon Nanotubes in a Centrifugal Field*. Langmuir, 2008. **24**(5): p. 1790-1795.
42. Kwon, T., et al., *Highly efficient exfoliation of individual single-walled carbon nanotubes by biocompatible phenoxylated dextran*. Nanoscale, 2013. **5**(15): p. 6773-8.
43. Yamakawa, H., *Viscoelastic Properties of Straight Cylindrical Macromolecules in Dilute Solution*. Macromolecules, 1975. **8**(3): p. 339-342.
44. Yao, Y., S. Luo, and T. Liu, *Determination of the Length, Diameter, Molecular Mass, Density and Surfactant Adsorption of SWCNTs in Dilute Dispersion by Intrinsic Viscosity, Sedimentation, and Diffusion Measurements*. Macromolecules, 2014. **47**(9): p. 3093-3100.
45. Luo, S., T. Liu, and B. Wang, *Comparison of ultrasonication and microfluidization for high throughput and large-scale processing of SWCNT dispersions*. Carbon, 2010. **48**(10): p. 2992-2994.
46. Luo, S. and T. Liu, *Structure–property–processing relationships of single-wall carbon nanotube thin film piezoresistive sensors*. Carbon, 2013. **59**(0): p. 315-324.
47. Luo, S., et al., *Variable Range Hopping in Single-Wall Carbon Nanotube Thin Films: A Processing–Structure–Property Relationship Study*. Langmuir, 2013. **29**(27): p. 8694-8702.
48. Mason, M. and W. Weaver, *The Settling of Small Particles in a Fluid*. Physical Review, 1924. **23**(3): p. 412-426.
49. Hagen, A. and T. Hertel, *Quantitative Analysis of Optical Spectra from Individual Single-Wall Carbon Nanotubes*. Nano Letters, 2003. **3**(3): p. 383-388.
50. Fujita, H., *Mathematical theory of sedimentation analysis*. Physical chemistry; a series of monographs,v. 111962, New York: Academic Press. 315 p.
51. Kozulic, B., *Models of gel electrophoresis*. Anal Biochem, 1995. **231**(1): p. 1-12.
52. Griess, G.A., et al., *The sieving of rod-shaped viruses during agarose gel electrophoresis. I. Comparison with the sieving of spheres*. Biopolymers, 1990. **29**(8-9): p. 1277-87.
53. Lerman, L.S. and H.L. Frisch, *Why does the electrophoretic mobility of DNA in gels vary with the length of the molecule?* Biopolymers, 1982. **21**(5): p. 995-997.
54. Slater, G.W., *DNA gel electrophoresis: the reptation model(s)*. ELECTROPHORESIS, 2009. **30**(1): p. 200900154.
55. Brochard Wyart, F. and P.G. de Gennes, *Viscosity at small scales in polymer melts*. The European Physical Journal E, 2000. **1**(1): p. 93-97.
56. de Gennes, P.G., *Motions of one stiff molecule in an entangled polymer melt*. J. Phys. France, 1981. **42**(3): p. 473-477.
57. Hertel, T., et al., *Diffusion Limited Photoluminescence Quantum Yields in 1-D Semiconductors: Single-Wall Carbon Nanotubes*. ACS Nano, 2010. **4**(12): p. 7161-7168.
58. Harrah, D.M. and A.K. Swan, *The Role of Length and Defects on Optical Quantum Efficiency and Exciton Decay Dynamics in Single-Walled Carbon Nanotubes*. ACS Nano, 2010. **5**(1): p. 647-655.
59. Siitonen, A.J., et al., *Dependence of Exciton Mobility on Structure in Single-Walled Carbon Nanotubes*. The Journal of Physical Chemistry Letters, 2010. **1**(14): p. 2189-2192.

